Structural Sizing of a 50-m-Tall Thermoplastic Composite Solar Array Truss Tower Structure for the Lunar South Pole

Andrew C. Bergan[1][0000-0002-3761-2129], Babak Farrokh[2], Arunkumar Satyanarayana[1], Will J. Grier[1], Kenneth N. Segal[2,3], John Chiu[2,4], and Sandi Miller[5]

[1] NASA Langley Research Center, Hampton, VA 23681, USA
[2] NASA Goddard Space Flight Center, Greenbelt, MD 20771, USA
[3] HelioSpace Corporation, Greenbelt, MD 20771, USA
[4] Actalent Corporation, Greenbelt, MD 20771, USA
[5] NASA Glenn Research Center, Cleveland, OH, 44135, USA

Abstract. At the lunar south pole, solar arrays elevated by truss towers are exposed to near continuous sunlight since the sun remains near the horizon. Recent studies suggest that tower heights on the order of 50 m are needed to meet the power requirements to support a sustained lunar presence. While eventually towers may be constructed using materials sourced in-situ, initially structural elements will likely be brought from the Earth, deployed, and assembled. Thermoplastic composites offer the benefit of high specific stiffness and strength properties along with welding for assembly joints, and therefore represent a promising material system for this application. The focus of this paper is on the structural sizing of such towers. A set of expressions based on beam theory are presented for preliminary sizing of the truss tower structure for strength and buckling. The loading condition that drives sizing is base excitation resulting from moonquakes. A point design, developed through finite element analysis, verifies the analytical sizing routine and shows the importance of joints. The results show a viable point design and highlight the factors most significant in the structural sizing.

Keywords: Thermoplastic composites, Lunar structures, Structural sizing.

1 Introduction

Since the sun stays near the horizon at the lunar south pole, lightweight tower structures that can elevate solar arrays can enable near continuous power in support of NASA's Moon to Mars Objectives [1]. However, developing a cost-effective capability for tall towers located near the lunar south pole is a significant structural engineering challenge. While smaller towers might rely on deployed masts [2, 3, 4], tower heights greater than ~25 m will likely be trusses [5]. NASA's Tall Lunar Tower (TLT) project [6] developed an approach for robotic structural assembly of a truss tower using riveting metallic connections at the ends of thermoset carbon fiber reinforced polymer (CFRP) square tubes. As part of NASA's Thermoplastics Development for Exploration

Applications (TDEA) project, the authors and coworkers developed a variant of the TLT design concept, with an all-thermoplastic CFRP design that can be assembled robotically by welding the members together at the truss nodes. This paper focuses on the tower structural analysis and sizing conducted by the TDEA team.

Data collected using seismic sensors during the Apollo missions [7, 8] and recent remote observations of geological features [9, 10, 11] suggest that strong seismic events are possible on the moon, and that such events should be considered in future Artemis mission plans [11]. Tall, slender towers with a concentrated mass at the top are particularly sensitive to ground shaking and so we assume seismic loads are the driving load case. We develop an analytical tower sizing routine, verify it against finite element model (FEM) results, and demonstrate its utility by 1) comparing the results obtained for different relevant material systems, and 2) assessing correlation with detailed analysis conducted for the TDEA point design.

The remainder of this paper is organized as follows. First, we describe the loading assumed to be representative of moonquakes. Then, we propose a set of equations for tower sizing by extending the work in [5, 6, 12] for the assumed moonquake loads. Next, we describe a solution procedure to solve the equations for the optimal tower sizing parameter and summarize initial verification of the results. Then, results from a parameter study are summarized to show the influence of tower member material. Finally, we summarize the detailed structural and thermal analysis performed for the TDEA project's point design to emphasize the key outcomes from the design-analysis iterations. The results show the significance of selected assumptions and help to identify potential improvements to the sizing routine, leading to rapid identification of feasible designs.

2 Moonquake Excitations and Tower Loads

The seismic events that result in the most severe shaking are called shallow moonquakes (SMQ) [7]. Some characteristics of moonquakes differ significantly from earthquakes. Recent simulations of SMQ events [9, 10, 11] provide a basis for ground excitations relevant for designing structures that can sustain such events. Watters et al. [11] provide a characterization of seismicity and preliminary assessment of slope stability for Artemis missions in the lunar south pole region. Ruiz et al. [13] reported a preliminary probabilistic seismic hazard assessment (PSHA) focused on the Apollo 17 landing site, which was later applied to habitat design [14]. The need for additional lunar seismic data has been recognized as a priority and is being addressed with the Farside Seismic Suite, which will provide long-lived seismic data [15].

The uniform hazard spectra (UHS) reported in [13] is used herein for tower structure design. The UHS for 2% and 10% probability of exceedance in 50 years (return periods $T_r = 2500$ years and 475 years, respectively) are reproduced in Fig. 1 in terms of the nondimensional base shear coefficient,

$$C_S = S_A(\omega_n)/g_M \tag{1}$$

and frequency. $S_A(\omega_n)$ is the spectral acceleration as a function of natural frequency and $g_M = 1.6$ m/s^2 is lunar gravity. C_S is a convenient parameter since the shear force

at the tower base is $V = C_S W$ where W is the weight of the tower. Since the tower structure designs considered herein can have natural frequencies, $f_n = \omega_n/(2\pi)$, that are relatively low, we assume the UHS curve can be linearly extrapolated as shown by the dashed line.

One important observation from the measurements made during the Apollo missions is that SMQ event duration can be greater than 1 hour. In that case, analysis using a shock response spectrum approach may be inadequate since a transient excitation is assumed. Therefore, we consider a harmonic excitation as a simplistic alternative. Since f_n is in the range of excited frequencies, resonance is assumed and so

$$C_S = \frac{\ddot{u}_g/g_M}{2\beta\sqrt{1-\beta^2}} \tag{2}$$

where $\ddot{u}_g$ is the ground acceleration and β is the damping factor. Since resonance is assumed, (2) is independent of frequency. In the TDEA project, $\ddot{u}_g/g_M = 0.15$ was assumed along with a typical structural damping $\beta = 3.3\%$. In this case, $C_S = 2.27$ which, when compared to Fig. 1, produces much higher loading for $f_n < 0.5$ Hz. Further analysis is needed to develop a more rigorous estimation for tower loads. In this paper, the results are calculated using (2) except as noted otherwise (for the purpose of highlighting the significance of the assumed loads).

The next two sections describe structural sizing methods that utilize the moonquake excitation described here. Since the dynamic loads vary with the tower stiffness, mass, and damping, an iterative approach is pursued.

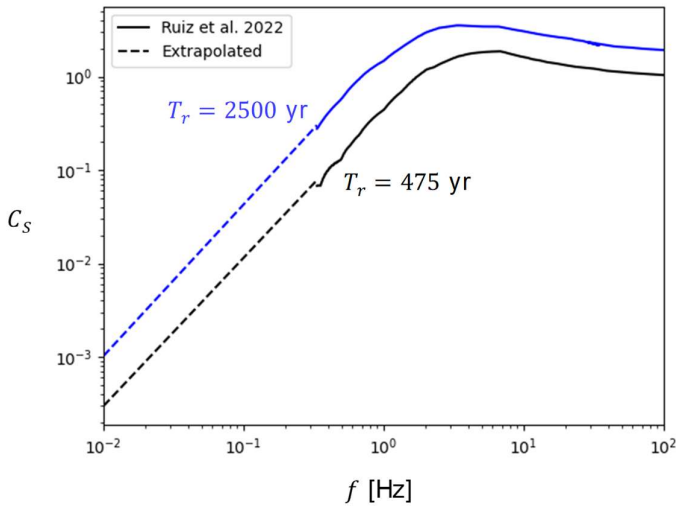

Fig. 1. Uniform hazard spectra from [13] replotted in terms of base shear coefficient.

3 Preliminary Structural Sizing

Preliminary sizing of truss towers is performed using a set of expressions based on beam theory and an iterative solution method to identify promising designs. The approach extends [5, 6, 12] by including base excitation (moonquake) loads and consideration for longeron strength. The method is presented in this section along with a design study.

3.1 Governing Equations

A prismatic truss tower is assumed with height, H, and square cross section with width, b (see Fig. 5 for a visual reference). The truss comprises four longerons located near the corners such that b is measured to the outside of the member cross section (overall width). The longerons have cross section area, A_L, and moment of inertia, I_L, and are constructed with material having a Young's modulus in the axial direction, E. The longerons are sized for positive margins on tower buckling, longeron buckling, and longeron strength. A residual for tower Euler buckling is calculated as

$$R_{TE} = \frac{\pi^2 E I_{\text{truss}}}{4H^2 FS} - M_{\text{eff}} g_M - M_{\text{eff}} S_{A,v} \tag{3}$$

where the first term is the buckling limit scaled by the factor of safety, FS, the second term is the static load due to gravity, the third term is additional dynamic load due to base excitation in the vertical direction. The effective mass M_{eff} is the mass of payload, M_{PL}, and the fraction of the mass of the truss M_{truss} lumped at the top of the tower [16]

$$M_{\text{eff}} = M_{PL} + 0.3 M_{\text{truss}} \tag{4}$$

M_{truss} is defined in [5] as

$$M_{\text{truss}} = A_L H \rho J \left(4 + 4\beta_{ah} + 5\sqrt{2}\beta_{ad}\right) \tag{5}$$

where ρ is the density of the material, β_{ah} and β_{ad} are area reduction factors for the horizontal and diagonal bracing members which may have more slender cross sections, and J is a nondimensional joint factor that represents the mass penalty of the joints. Eqn. (5) is independent of b, since cubic bays are assumed. Herein, it is assumed that $\beta_{ah} = \beta_{ad} = 0.7$ and $J = 1.3$ following [5]. The moment of inertia of the truss $I_{\text{truss}} = 4I_x + A_L b^2$ where I_x is the moment of inertia of the longeron about the axis that minimizes I_{truss}. In [5], it is assumed that I_x is negligible. Vertical acceleration due to moonquake excitation is included in the third term of (3) since SMQ events are thought to induce horizontal and vertical ground accelerations with similar magnitudes, e.g. [9]. Hence for the UHS, we assume $S_{A,v} = S_A$ and evaluate using the extensional natural frequency, $\omega_{n,e}$. For harmonic ground motion, $S_{A,v}$ can be calculated assuming $\ddot{u}_{go,v} = \ddot{u}_{go}$ and $S_{A,v} = \ddot{u}_{go,v} R_{d,v}$ where $R_{d,v}$ is a standard transfer function (see, e.g. [17])

$$R_{d,v} = \frac{1}{{\omega_{n,e}}^2} \frac{1}{\sqrt{(1-r^2)^2 + (2\beta r)^2}} \tag{6}$$

with the frequency ratio r calculated using $\omega_{n,e}$ as

$$r = \omega/\omega_{n,e} = \omega\left(\frac{4A_L E}{M_{\text{eff}}H}\right)^{-1/2} \tag{7}$$

For most practical designs, $r \ll 1$, $\omega_{n,e}\sim 1$, and therefore $R_{d,v} \leq 1$. Herein, $R_{d,v} = 1$ is used as a conservative assumption.

The bending mode natural frequency of the tower with payload mass M_{PL} is obtained from [18] as

$$\omega_n = \sqrt{\frac{\frac{\pi^4 EI_{\text{truss}}}{32H^3} - g_M\left(\frac{\pi^2(2M_{PL} + M_{\text{truss}}) - 4M_{\text{truss}}}{16H}\right)}{M_{PL} + (3\pi - 8)M_{\text{truss}}/2\pi}} \tag{8}$$

where the numerator is the bending stiffness of the tower, and the denominator is the tower mass where the factor 0.23 is used to get the effective truss mass at the tip (see [16] or [18]). In (8), vertical acceleration due to moonquakes is ignored.

To calculate residuals for strength and buckling of the longerons, the maximum compressive force in the longerons F_L is assumed to occur near the base of the tower. F_L is the sum of the force due to axial compression of the tower (last two terms in (3)) and the force due to the bending moment resulting from horizontal base excitation

$$F_L = \frac{M_{\text{eff}}}{4}(g_M + \ddot{u}_v) + \frac{H}{2b}C_S(\omega_n)(M_{PL} + 0.23M_{\text{truss}})g_M \tag{9}$$

The first term is negligible in most cases. Using (9), residuals for longeron strength and buckling are

$$R_{LS} = \frac{X_c A_L}{FS} - F_L \tag{10}$$

$$R_{LE} = \frac{\pi^2 E I_L}{b^2 FS} - F_L \tag{11}$$

respectively, where X_c is the compressive strength of the longeron material and I_L is assumed to be calculated about the axis that produces a minimum. In the first term in (11), Euler buckling load for the longeron is calculated assuming the truss comprises square bays having height b and free rotation of the truss nodes so the end conditions are pin-pin, which should be a conservative assumption since the joint has some stiffness.

3.2 Solution Method

With the residuals defined in (3), (10), and (11), the sizing of the truss is defined by longeron cross sectional parameters A_L and I_L, and the tower width b. The problem is to minimize these residuals subject to constraining to A_L, I_L, and b to be practical values (i.e., greater than some small positive value) where we assume that near zero margin minimizes the structural mass.[1] The values for β_{ah} and β_{ad} are considered fixed

[1] A more conventional approach in the truss optimization literature is to minimize the mass subject to constraints defining the design criteria. Since buckling introduces a nonlinear

parameters. Since small positive residuals (positive margin) are much more desirable than small negative residuals, the total residual is calculated as

$$\mathbb{E} = \sum_{i=TE,\,LE,LS} \left[R_i\left(k_s + \mathbb{H}(-R_i)(1-k_s)\right)\right]^2 \tag{12}$$

where $\mathbb{H}(x)$ is the Heaviside operator and k_s is a small positive number such that the error scales $1/k_s$ slower when the residual is positive. The solution is obtained by minimizing (12) using the dual annealing method [19] available in SciPy [20], which is a stochastic global optimization algorithm that explores the solution space by selecting the next trial point close to the current one if the objective function is within a tolerance that decreases through the solution history. Bounds are selected to aid the solution routine based on engineering judgement and trial-and-error to limit trial solutions to practical values. The results described below are local minima not limited by arbitrary bounds.

3.3 Verification and Demonstration

Initial verification of the proposed method is obtained by comparison of the longeron strength and buckling results with a FEM. The FEM is constructed with beam elements representing the truss members for $H = 51$ m, $b = 1.5$ m, and with nonstructural mass for the payload $M_{PL} = 1000$ kg. The truss connectivity is the one identified from the trade study in [12] (see Fig. 5). The longerons are assumed to have symmetric L-shaped cross sections with flange thickness $t = 5$ mm and a flange length, L, of 50 mm ($L/t = 10$ assumed so that flange buckling can be ignored). Nonstructural mass is included at the joints corresponding to $J = 1.3$. The material is assumed to be a zero-dominated laminate of TC1225 T700/LM-PAEK thermoplastic composite having longitudinal modulus $E = 92$ GPa, density $\rho = 1600$ kg/m^3, and compressive strength $X_c = 350$ MPa [21]. The FEM was fixed at the base and several analyses were run. The bending and axial frequencies were obtained from a modal analysis and found to be 0.22 Hz and 8.6 Hz, which are reproduced by the analytical expressions within 2%. An eigenvalue buckling analysis was used to analyze tower buckling and yielded a buckling load that is calculated within 1% using Euler buckling from the first term on the right-hand-side (RHS) of (3). Then, a dynamic analysis was conducted for harmonic base excitation sweep from 0.1 to 10 Hz with $\ddot{u}_g/g_M = 0.15$ and $\beta = 3.3\%$, which produced a maximum tip deflection of 1.9 m at resonance. Using this deflection as representative of the static equivalent load, the maximum longeron load was obtained from a quasi-static analysis and is 5% of the value calculated by (9). The longeron buckling load from the FEM is about twice the value obtained from the first term on the RHS of (11), which is not surprising since the joint is rigid in the FEM and its rotation is resisted by the diagonal and horizontal bracing members whereas the longeron is treated as having pinned ends in (11). Considering the joint stiffness is likely overestimated by the beam-element FEM, the conservatism in (11) is assumed acceptable.

---

constraint, the numerical solution is challenging, and some type of linearization is usually required, e.g., [14]. The present approach circumvents this issue.

The total residual in (12) is calculated using the model parameters defined above ($H = 51.3$ m, $L/t = 10$, $M_{PL} = 1000$ kg, $J = 1.3$, $E = 92$ GPa, $X_c = 350$ MPa, $\rho = 1600$ kg/m^3, $\beta = 3.3\%$, $FS = 1.5$) for a range of t and b and visualized as a contour plot in Fig. 2 for harmonic ground motion (a) and the UHS with $T_r = 475$ years (b). In both cases there is a clear local minimum, which is found by the optimization routine (cyan-colored circle). The curves corresponding to zero residuals in (3), (10), and (11), are shown with the brown, pink, and olive-colored markers. These curves indicate zero margin with positive margin being above and to the right of the curves. For harmonic ground motion, longeron buckling and strength size the structure whereas for the UHS, tower Euler buckling and longeron buckling size the structure (for this set of parameters). For the UHS load case, the longeron strength margin R_{LS} is relatively independent of b since the longeron load F_L is relatively insensitive to b. R_{LS} happens to be near zero for this set of parameters, but can drive sizing when other parameters are specified. The optimal design for the UHS loading has a larger b and smaller t and so it is lighter. Using $T_r = 2500$ years, b is about the same but t increases by about 30%. Zero margin designs show rather gradual increases in t when changing b slightly from the optimal value. When b is reduced significantly to around 0.3 m, the required t increases rapidly.

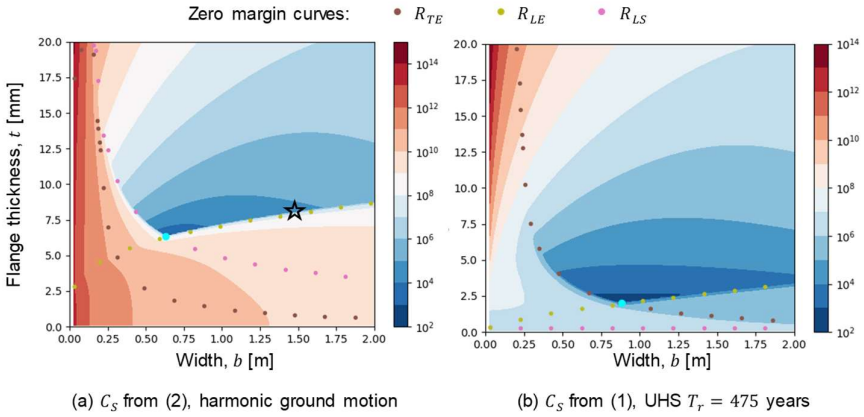

Fig. 2. Contour plots of total residual, E, over a range of t and b for the two different assumed ground motion conditions. The lines show curves of zero residual. The cyan circles show the optimal structure, obtained by minimizing (12). The star shows the TDEA point design.

With the model parameters defined above, the truss mass, natural frequency, and maximum tip displacement are calculated for a range of t and b and visualized as a contour plot in Fig. 3. The results for M_{truss} calculated using (5) and shown in Fig. 3a visually illustrate that $M_{truss} \propto t^2$, and that M_{truss} is independent of b. The natural frequency (8) of the tower increases with both t and b, remaining relatively low for the range of values considered, as shown in Fig. 3b. When the numerator of (8) is negative, Euler buckling occurs due to gravity and ω_n is imaginary; this region is shown in white in Fig. 3b. The maximum tip displacement, $u_{\max}$, is estimated by $u_{\max} = C_S/(g_M {\omega_n}^2)$ with C_S calculated using (2). The $u_{\max}$ are relatively large values, as shown in Fig. 3c,

where the results are truncated at $u_{\max}/H = 0.1$ since small deformations are assumed. Herein, no constraint is placed on maximum tip displacement. However, adding a design constraint for dimensional stability is an obvious extension of this work and would lead to designs with larger b or alternative design concepts such as guy wires (see, e.g., [4]).

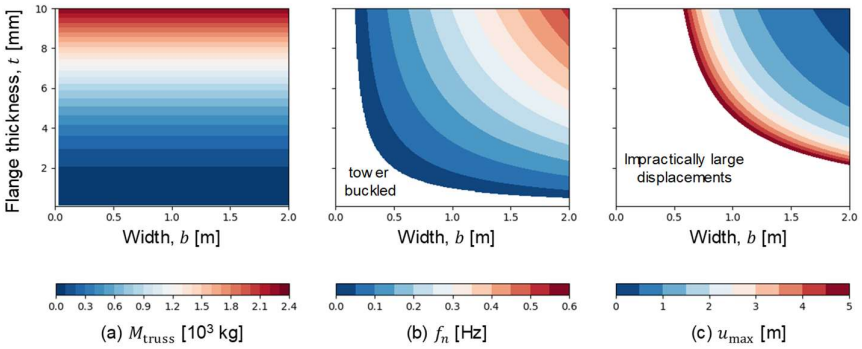

Fig. 3. Contour plots of (a) tower structural mass, (b) natural frequency, and (c) maximum tip displacement illustrate trends with the sizing parameters, t and b.

3.4 Preliminary Sizing of a 50-m-Tall Tower

The tower sizing routine is applied to size a 50-m-tall tower using five different materials and three different payloads M_{PL} to evaluate the significance of payload mass and material selection on the tower dimensions and mass. The materials include three CFRP composites and two aluminums, with input properties listed in Table 1. The TC1225 material is a T700/LM-PAEK thermoplastic CFRP material used in the TDEA project. The layup is a zero-biased "hard" layup. A second variant of TC1225 is included with a quasi-isotropic (QI) layup. The third CFRP material, HM63/8552, has high-stiffness fibers with a zero-biased "hard" layup and an epoxy resin. The resin properties are not required for this sizing, so the results for HM63/8552 are likely representative of what might be achieved with high-stiffness fibers and a thermoplastic resin. To the authors' knowledge, there is no commercially available high-stiffness fiber thermoplastic composite material system, and no material property data are available for such a material. The aluminum 7075-T6 represents an aerospace grade aluminum while AL 1100 is meant to represent aluminum produced in-situ on the lunar surface. The tower size parameters are the tower width, b, and longeron cross section thickness, t, with symmetric L-shaped cross sections with $L/t = 10$ held constant. A harmonic acceleration with $\ddot{u}_g/g_M = 0.15$ is used. For the composite materials and AL 1100, $FS = 1.5$, and for AL 7075-T6, $FS = 1.4$ is applied. The results are summarized in Fig. 4. From left to right, each bar corresponds to a different tower configuration (material and payload mass). The three plots show the results of the sizing for member thickness t, tower width b, and truss mass M_{truss}. Overall, the trends show t and M_{truss} increasing with payload and more flexible materials. Note that tower width b increases with stiffer

materials since square truss bays are assumed and stiffer materials reach zero margin in (11) at larger values of b. The tower widths are omitted for AL 1100 since the values are much higher than for the other materials (e.g., 4.5 m for $M_{PL} = 1000$ kg). Using TC1225 hard in place of AL 7075-T6 yields a 41% reduction in M_{truss}. The high-stiffness fiber material, HM63/8552, provides an additional 9% mass reduction. M_{truss} increases by about 10 times for towers made with AL 1100.

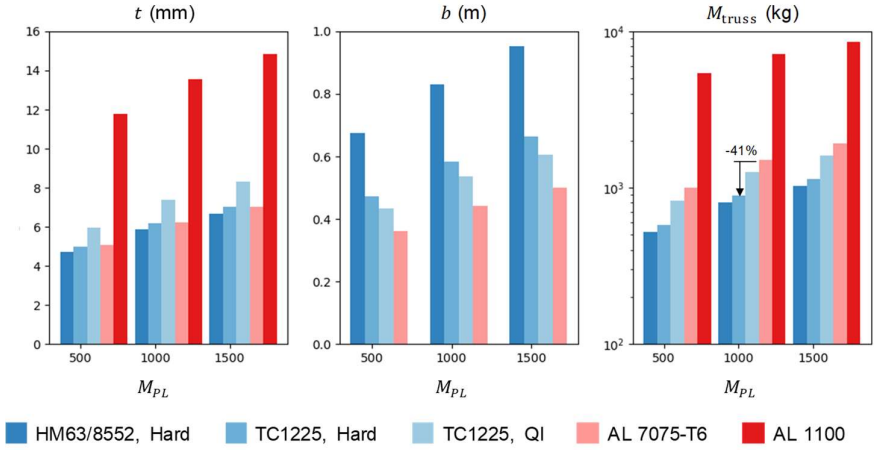

Fig. 4. Sizing results for 'L' section designs for different materials and payload masses.

Table 1. Material properties for sizing study.

Material	E [GPa]	Strength [MPa]	ρ [kg/m^3]	Reference
HM63/8552	162.0$^{\alpha}$	300$^{\beta}$	1600	[22]
TC1225, Hard	92.9$^{\alpha}$	393$^{\gamma}$	1600	[21]
TC1225, QI	45.0$^{\alpha}$	324$^{\gamma}$	1600	[21]
AL 7075-T6	71.7	538$^{\delta}$	2700	[23]
AL 1100	68.9	24$^{\varepsilon}$	2700	[23]

$^{\alpha}$ Calculated using classical lamination theory from reported mean values
$^{\beta}$ Estimated
$^{\gamma}$ Mean value
$^{\delta}$ Ultimate
$^{\varepsilon}$ Yield

4 Detailed Structural Analysis for the TDEA Point Design

In the TDEA project, detailed structural design and analysis were performed for a point design (PD). The PD served to focus development work on the joints around a particular design and led to coupon and sub-element structural substantiation tests.

The PD was developed using a set of design requirements and assumptions. The pertinent design requirements are summarized in Table 2. Many additional considerations that would be required for a complete system, such as interface with robotic

manipulators for assembly and thermal cycling, are not addressed due to the limited scope of the study. The design was also constrained by the several assumptions as follows. The tower cross-section is square and prismatic with width $b = 1.5$ m. The width was selected with some conservatism using an early version of the sizing model described above. The truss connectivity from [12] is adopted without further assessment of alternatives. Also following [12], the joint design comprises a joint splice plate (JSP) at each truss node to which truss members are welded (on the lunar surface) for tower assembly. TDEA considered four commercially available thermoplastic composite prepreg materials and selected TC1225 T700G/LM-PAEK for the PD based on available material property data. The truss parts are designed for manufacturing by automated fiber placement (AFP) with autoclave consolidation. An 'L'-shaped cross section is assumed for all the truss members as above. The 'L'-shaped cross section enables a design that can be packaged compactly during launch, is readily compatible with several TPC weld techniques, and is manufacturable with AFP.

The PD is shown in Fig. 5. For the dimensions and truss connectivity selected, the 51-m-tall tower comprises seventeen repeating unit cells (RUC). Design and analysis were iterated to achieve positive margins, with focus on the cross-section dimensions of the truss members, and the joint geometry at the truss node locations. The rest of this section describes the key outcomes from the design-analysis iterations for the truss members and joints.

Table 2. Design requirements used for the TDEA PD.

	Requirement name	Parameter	Reference
1	Positive margin of safety	> 0	[24]
2	Composite material FS	1.5 uniform material 2.0 discontinuities	[24]
3	Payload mass	$M_{PL} = 1000$ kg	Assumed
4	Base interface	Fixed base, 4 corners	[6]
5	Thermal environment	Survive predicted extreme temperatures	
6	Gravity load	$g_M = 1.62$ m/s^2	
7	Dynamic loads	Harmonic base excitation, $\ddot{u}_g/g_M = 0.15$	Assumed

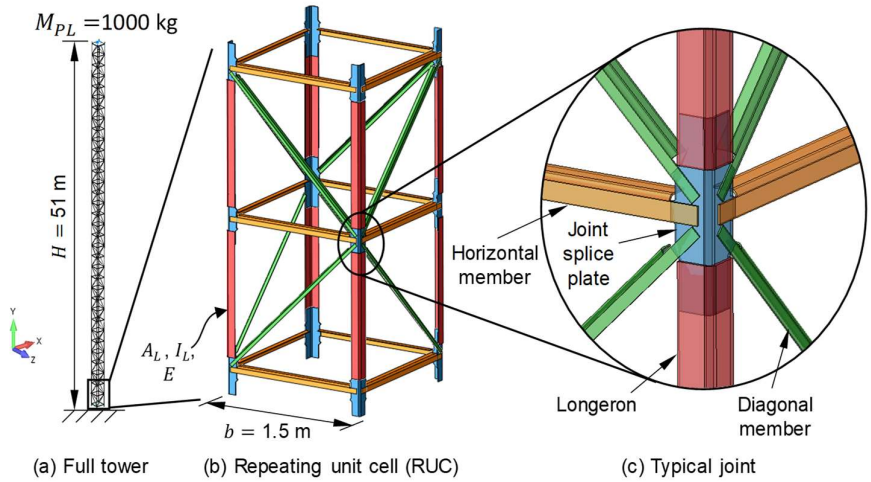

Fig. 5. TDEA point design. The joint region is shown with transparency so that the overlap (welded) regions are visible.

4.1 Truss Members

A FEM of the PD was built in Femap [25] and analyzed with Simcenter Nastran [26] with around 560,000 shell elements representing the truss members and JSPs, having a typical element edge length of 13 mm. At joint locations, the truss members connect to a JSP with overlapped elements and shared nodes. Since the joint geometry is modeled in this shell element FEM, no additional nonstructural joint mass is included for the joints. The laminate properties for the truss parts were calculated based on lamina properties (mean values) reported in [21] for the layups determined through design-analysis iteration. The material 0°-direction is along the axis of the 'L'-shaped members. The tip loads (or concentrated mass element) and fixed-base boundary conditions are implemented at single nodes at the top and bottom and are connected to the shell mesh with RBE2 multipoint constraints. Results were evaluated 1 RUC above the fixed base since the actual base boundary condition is not defined or modeled.

The analytical sizing model suggests that the PD is driven by longeron strength and buckling, as shown in Fig. 2a. The FEM was analyzed for both strength and buckling, and, in the cases run, the truss member sizing was driven by buckling. In the buckling analysis, the tower is subject to a preload that is an equivalent static tip load obtained from the dynamic base excitation analysis.

Design-analysis iterations produced a design with positive margin on buckling. The initial and final cross-sectional dimensions of the four truss parts are summarized in Table 3. The initial section dimensions were selected somewhat arbitrarily, without the benefit of the sizing method described above. The final dimensions reflect changes to achieve positive margin for longeron buckling and introduction of a corner radius, R, for manufacturability. Using the analytical sizing routine described above for $b =$

1.5 m, the flange thickness $t = 8$ mm (star in Fig. 2a), which agrees well with the final result obtained using the FEM. In the final design of the horizontal and diagonal members, $\beta_{ah} = 0.45$ and $\beta_{ad} = 0.25$, which are much lower than the initial assumption of $\beta_{ah} = \beta_{ad} = 0.7$. Extension of the analytical sizing framework to account for the stiffness of the bracing members may help arrive at better values for bracing member sizing during preliminary design.

Table 3. PD truss part dimensions (mm).

		Longeron	JSP	Horizontal	Diagonal
L	Initial	50	50	50	30
	Final	98	90	69	49
t	Initial	5	3	5	3
	Final	8.2	7.1	5.2	4.1
R	Initial	0	0	0	0
	Final	12.7	12.7	12.7	12.7

Including the corner radius in the FEM led to a need for increased L and t to obtain positive margins. In other words, practical values for the corner radius have a nonnegligible effect on the member's moment of inertia. This is verified by calculating I_L and I_{truss} as a function of the corner radius, as shown in Fig. 6. With these results, future preliminary sizing efforts can incorporate the corner radius.

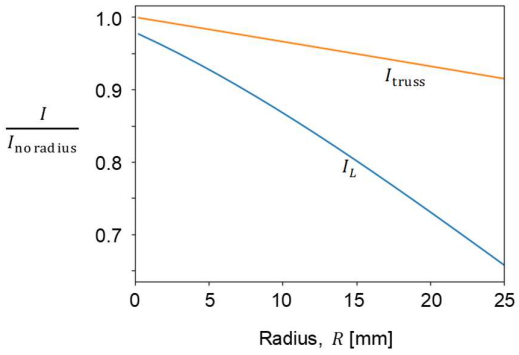

Fig. 6. Effect of 'L' section corner radius on moments of inertia. These results use the cross-section parameters from the TDEA longeron design (final).

4.2 Joints

Two aspects of the joint design are discussed here: the joint stiffness and joint strength. The joint stiffness is relevant to the longeron buckling margin. In the final joint design, the truss members overlap the JSP, extending toward their intersection, and terminating just short of interference (see Fig. 5c). The extended overlaps add stiffness to the JSP. In the case of the horizontal and diagonal members, the overlap length

is more than required for joint strength. Earlier design iterations with tabs on the JSP position the joint away from the corner for easier access for welding, but result in local buckling modes, for example as shown in Fig. 7a. Following these observations, an alternative design was explored with the orientation of the horizontal and diagonal members rotated so that both flanges of 'L' could extend the full length of the members, as shown in Fig. 7b, however, this variation did not improve the buckling margin enough to lead to a significant mass reduction.

The joint strength also must be addressed to show positive margin for the joint. Each of the up to eight welded connections at the JSP are analyzed separately using detailed FEMs with cohesive elements to predict failure of the welded interface using Abaqus. The longeron-JSP connection is most highly loaded and so it is addressed here (a similar approach was applied for the other joints). An overview of the detailed FEM is shown in Fig. 8a. The longeron and JSP are modeled with solid shell elements (SC8R) with both having $L = 70$ mm and $t = 7$ mm. The two parts are connected by a layer of zero-thickness cohesive elements (COH3D8) in the two weld areas. A weld stand-off is included around the perimeter of the weld area and is modeled with a contact condition. The cohesive interface used strength and toughness properties corresponding to the TC1225 interlaminar properties [27] since properties calibrated to welds were not available. Simplified boundary conditions representing uniaxial loading along the joint were applied, as shown in Fig. 8a. The analysis was run in Abaqus/Explicit for different overlap lengths L_w. The predicted peak loads normalized by the design limit load (DLL) are plotted vs. L_w five overlap lengths in Fig. 8b. The results show that the design criterion of 2 DLL (FS = 2 for discontinuity) is met with $L_w \geq 83$ mm. The results suggest that the joint strength plateaus around $L_w = 2L$. In the preliminary sizing described previously, the only consideration for the joints is a joint mass penalty J. Since the JSP and longerons use the same material and have similar cross-sectional dimensions, additional mass at the joints is assumed to be equal to the overlapped length. For the case where $L_w = 2L$, $L = 70$ mm, and $b = 1.5$ m, each node has two joints, so $J = 4L/b + 1 = 1.19$, which is lower than the assumption of $J = 1.3$ used in the preliminary sizing and should be updated in future work.

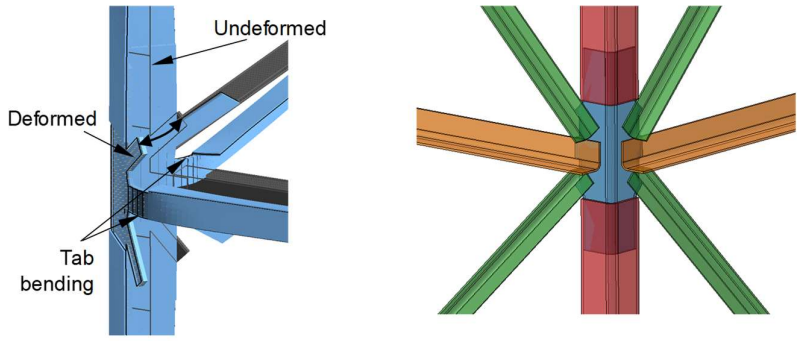

(a) Local buckling mode (twisting)

(b) Alternative orientation of horizontal and diagonal members

Fig. 7. Alternative configuration with rotated, unnotched horizontal and diagonal members.

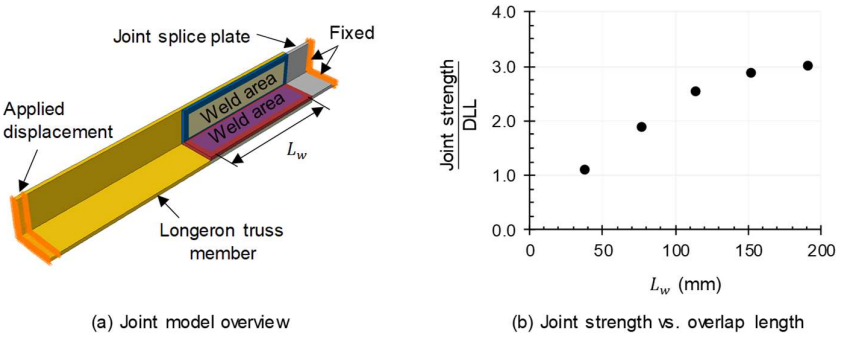

Fig. 8. TDEA PD joint strength model and analysis results.

5 Thermal Structural Analysis

The PD was interrogated further by thermal structural analysis. A thermal model was developed using Thermal Desktop to simulate the thermal environments present at the surface of lunar south pole. The tower is located on the Shackleton Connecting Ridge at 89.47°S, 222°E with an elevation of 1940 m as representative based on previous solar illumination studies [28, 29] The tower is modeled with 33,000 nodes, and placed 2 m above (no conduction) a flat circular lunar surface ground plane[2] modeled with 200 nodes as shown in Fig. 9a. The ground plane was geometrically sized (r in Fig. 9a) relative to local lunar surface elevation, tower height, and minimum solar elevation angle at which incident radiation is imparted onto the tower. A time-varying solar vector orbit table relative to the specified location is applied via JPL Horizons ephemeris data [30] for an arbitrary date range of 6/1/25 to 6/1/26. Lunar orbital and surface properties obtained from [31] are used. Solar flux, albedo, regolith infrared (IR) emissivity, and regolith solar absorptivity are assumed to be constant at 1367 W/m^2, 0.160, 0.965, and 0.840, respectively [31]. Lunar surface boundary temperature profiles obtained from Lunar Reconnaissance Orbiter (LRO) flight data [32] are represented with a polynomial fit. Local terrain and its impacts on incident solar illumination and surface temperature were not included. The resulting solar elevation angle and surface temperature are shown in Fig. 9b. The truss members are modeled to match those of the structural FEM. The optical properties of TC1225 were obtained via coupon testing, which resulted in an IR emissivity of 0.832 and solar absorptivity of 0.892. Temperature dependent specific heat [33] and thermal conductivity measured by the TDEA project are used. Thermal results were assessed over the complete analyzed date range. A worst case for structural-thermal deformation was selected where the bottom most RUC was at minimum temperature (-197°C) and the rest of the tower was exposed to sunlight (max temperature 85°C). Nodal temperature values from the thermal model were mapped to the structural FEM mesh and then the model was analyzed using a reference

[2] In other words, the lander or base, which may be conducting or insulating, is not considered.

initial temperature of -180°C and constant values for coefficient of thermal expansion. The results show a maximum displacement of 8 mm, which is negligible compared to the seismic loads. Qualitatively, the results suggest that the horizontal joint may be the most susceptible to thermal deformation induced loads, which is expected since this joint has the most significant mismatch in layups. Future analysis should consider the role of the welding process and local thermal structural analysis of the joints.

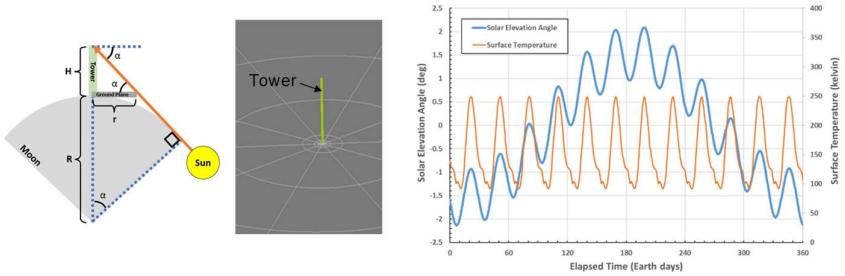

(a) Tower and simplified lunar ground plane (b) Solar elevation angle and lunar surface temperature

Fig. 9. Thermal model overview.

6 Summary

In this paper, an approach was proposed for structural sizing of vertical solar array truss towers subjected to base excitation from moonquakes. The analytical method extends previously developed sizing expressions based on beam theory [5, 6, 12]. The structural sizing accounts for Euler buckling of the tower and longerons and strength of the longerons. Verification of the sizing routine was performed through comparison with FEM results and shows good agreement. A parametric study was conducted to assess the role of material selection and the results show that high-stiffness materials such as CFRP save significant mass compared with AL 7075-T6. Considering assumed properties for in-situ sourced aluminum, towers constructed from such material will likely require an order of magnitude more massive structure and perhaps different truss architecture. The TDEA project point design is shown structurally feasible based on the available analysis results. The point design highlights the importance of joint stiffness and shows that CFRP welded joints can be a structurally efficient option.

Acknowledgements

The authors gratefully acknowledge the TLT team for stimulating discussions and sharing data and models. This work was funded by NASA's Space Technology Mission Directorate, Game Changing Development Program.

References

[1] NASA, "Moon to Mars Objectives," September, 2022.

[2] R. Pappa, C. Taylor, J. Warren, M. Chamberlain, S. Cook, S. Belbin, R. Lepsch, D. Tiffin, B. Doggett, M. Mikulas, I. Wong, D. Long, D. Steinkoening, A. Pensado, J. Blandino and J. Haste, "Relocatable 10 kW Solar Array for Lunar South Pole Missions," NASA/TM-20210011743, 2021.

[3] C. Taylor and R. Pappa, "Vertical Solar Array Technology Project," in *GCD Annual Review*, San Antonio, TX, 2023.

[4] J. G. Daye, A. J. Lee and J. M. Fernandez, "Structural Architectures for Self-Erecting Lunar Towers," in *AIAA SCITECH 2023 Forum, American Institute of Aeronautics and Astronautics*, 2023.

[5] W. R. Doggett, J. Heppler, M. K. Mahlin, R. Pappa, J. Teter, K. Song, B. White, I. Wong and M. Mikulas, "Towers: Critical Initial Infrastructure for the Moon," in *AIAA SciTech Forum*, National Harbor, MD, 2023.

[6] K. Song, M. Mikulas, M. K. Mahlin and J. T. Cassady, "Sizing and Design Tool for Tall Lunar Tower," in *AIAA SciTech Forum*, National Harbor, MD, 2023.

[7] C. Nunn, R. Garcia, Y. Nakamura, A. Mausiak, T. Kawamura, D. Sun, L. Margerin, R. Weber, M. Drilleau, M. Wieczorek, A. Khan, A. Rivoldini, P. Lognonné and P. Zhu, "Lunar Seismology: A Data and Instrumentation Review," *Space Science Reviews,* vol. 216, no. 5, p. 89, 2020.

[8] Y. Nakamura, G. V. Latham and H. J. Dorman, "Apollo Lunar Seismic Experiment—Final Summary," *Journal of Geophysical Research: Solid Earth,* vol. 87, no. S01, pp. A117–A123, 1982.

[9] T. R. Watters, R. C. Weber, G. C. Collins, I. J. Howley, N. C. Schmerr and C. L. Johnson, "Shallow Seismic Activity and Young Thrust Faults on the Moon," *Nature Geoscience,* vol. 12, no. 6, pp. 411-417, 2019.

[10] R. Mohanty, S. P. Kumar, S. T. G. Raghukanth and K. J. P. Lakshmi, "The Long-Lived and Recent Seismicity at the Lunar Orientale Basin: Evidence From Morphology and Formation Ages of Boulder Avalanches, Tectonics, and Seismic Ground Motion," *Journal of Geophysical Research: Planets,* vol. 125, no. 12, pp. 1-29, 2020.

[11] T. R. Watters, N. C. Schmerr, R. C. Weber, C. L. Johnson, E. J. Speyerer, M. S. Robinson and M. E. Banks, "Tectonics and Seismicity of the Lunar South Polar Region," *The Planetary Science Journal,* vol. 5, no. 1, p. 22, 2024.

[12] K. Song, A. Stark, R. Amundsen, M. Mikulas, M. K. Mahlin and J. T. Cassady, "Sizing, Buckling, and Thermal-Structural Analysis of Tall Lunar Tower," in *ASCEND 2023*, Las Vegas, NV, 2023.

[13] S. Ruiz, A. Cruz, D. Gomez, S. J. Dyke and J. Ramirez, "Preliminary Approach to Assess the Seismic Hazard on a Lunar Site," *Icarus,* vol. 383, p. 115056, 2022.

[14] C. Patiño, S. Ruiz, D. Gomez, A. Cruz, S. J. Dyke and J. Ramirez, "Seismic Assessment of a Long-Term Lunar Habitat," *Acta Astronautica,* vol. 214, pp. 414–426, 2024.

[15] NASA JPL, "The Farside Seismic Suite," [Online]. Available: https://www.jpl.nasa.gov/missions/the-farside-seismic-suite. [Accessed 14 6 2024].

[16] S. S. Rao, Mechanical Vibrations, Pearson Prentice Hall, 2003.

[17] P. H. Wirsching, T. L. Paez and K. Ortiz, Random Vibrations: Theory and Practice, Courier Corporation, 2006.

[18] A. de M. Wahrhaftig, R. M. L. R. F. Brasil and J. M. Balthazar, "The First Frequency of Cantilevered Bars with Geometric Effect: A Mathematical and Experimental Evaluation," *Journal of the Brazilian Society of Mechanical Sciences and Engineering,* vol. 35, no. 4, pp. 457-467, 2013.

[19] Y. Xiang and X. G. Gong, "Efficiency of Generalized Simulated Annealing," *Physical Review,* vol. 62, p. 4473, 2000.

[20] SciPy documentation, v1.13.0, "scipy.optimize.dual_annealing," [Online]. Available: https://docs.scipy.org/doc/scipy/reference/generated/scipy.optimize.dual_annealing.html. [Accessed 3 May 2024].

[21] E. Lian, "Medium Toughness PAEK Thermoplastics Toray (Formerly TenCate) Cetex® TC1225 (LM PAEK) T700GC 12K T1E Unidirectional Tape 145 gsm 34% RC Qualification Material Property Data Report, CAM-RP-2019-036 Rev A," NIAR, Wichita, KS, 2021.

[22] Hexcel, "HexTow HM63 Carbon Fiber," 2023. [Online]. Available: https://www.hexcel.com/user_area/content_media/raw/HM63_Aerospace_HexTow_DataSheet.pdf. [Accessed 20 5 2024].

[23] The Engineering ToolBox (2008), "Aluminum Alloys - Mechanical Properties," [Online]. Available: https://www.engineeringtoolbox.com/properties-aluminum-pipe-d_1340.html. [Accessed 20 5 2024].

[24] NASA Technical Standard, "Structural Design and Test Factors of Safety for Spaceflight Hardware, NASA-STD-5001B w/ change 3," 2022.

[25] Siemens Digital Industries Software, "FEMAP, version 2301 MP1," [Online]. Available: https://www.sw.siemens.com/en-US/.

[26] Siemens Digital Industries Software, "Simcenter Nastran, version 2212," [Online]. Available: https://www.sw.siemens.com/en-US/.

[27] Toray Advanced Composites, "Toray Cetex TC1225 Product Data Sheet," [Online]. Available: https://www.toraytac.com/media/3bd72fac-0406-48e4-bfc4-2ffd2398ac0c/fxj5OQ/TAC/Documents/Data_sheets/Thermoplastic/UD%20tapes,%20prepregs%20and%20laminates/Toray-Cetex-TC1225_PAEK_PDS.pdf. [Accessed 11 6 2024].

[28] E. Mazarico, G. A. Neumann, D. E. Smith, M. T. Zuber and M. H. Torrence, "Illumination Conditions of the Lunar Polar Regions Using LOLA Topography," *Icarus,* vol. 211, no. 2, pp. 1066–1081, 2011.

[29] J. M. Raya Armenta, N. Bazmohammadi, D. Saha, J. C. Vasquez and J. M. Guerrero, "Optimal Multi-Site Selection for a PV-Based Lunar Settlement Based on a Novel Method to Estimate Sun Illumination Profiles," *Advances in Space Research,* vol. 71, no. 5, pp. 2059–2074, 2023.

[30] NASA JPL, "Solar System Dynamics," [Online]. Available: https://ssd.jpl.nasa.gov/.

[31] NASA, "Cross-Program Design Specification for Natural Environments (DSNE), SLS-SPEC-159, Rev I," NASA, 2021.

[32] Washington University in St. Louis, "Planetary Data System (PDS) Geosciences Node," [Online]. Available: https://pds-geosciences.wustl.edu/.

[33] C. Ageorges, L. Ye, Y.-W. Mai and M. Hou, "Characteristics of Resistance Welding of Lap Shear Coupons. Part I: Heat transfer," *Composites Part A: Applied Science and Manufacturing,* vol. 29, no. 8, pp. 899-909, 1998.